

Granular jamming and rheology in microgravity

Qing Yu^{1,2,3}, Thorsten Pöschel¹, and Olfa D'Angelo^{*4,1}

¹Institute for Multiscale Simulation, Universität Erlangen-Nürnberg, Cauerstraße 3, 91058 Erlangen, Germany

²Technical University of Munich (TUM), TUM School of Natural Sciences, Department of Chemistry, 85748 Garching, Germany

³Research Group Electromobility and Learning Systems, Technische Hochschule Ingolstadt, 85049, Germany

⁴Institut Supérieur de l'Aéronautique et de l'Espace (ISAE-SUPAERO), Université de Toulouse, Toulouse, France

Understanding how granular materials behave in low gravity is crucial for planetary science and space exploration. It can also help us understand granular phenomena usually hidden by gravity. On Earth, gravity dominates granular behavior, but disentangling its role from intrinsic particle interactions is challenging. We present a series of compression and shear experiments conducted in microgravity using the Center of Applied Space Technology and Microgravity (ZARM) drop tower and GraviTower Bremen (GTB). Our in-house developed experimental setup enables precise measurement of packing density and *in-situ* shear stress via a Taylor-Couette rheometer. We find that the jamming transition occurs at lower packing density in microgravity than on Earth, confirming that gravity promotes densification. Rheological measurements further reveal that in microgravity, the lack of a secondary force field and predominance of cohesive interparticle forces increase the stress needed for granular media to flow. These findings highlight gravity's dual role in enhancing both compaction and flow, and demonstrate the need for tailored granular models, valid in low- and microgravity environments.

I. INTRODUCTION

From celestial bodies to fine powders, a wide array of materials are *granular*: a collection of particles, too large for thermal fluctuations, too loosely bound together to form a solid. Because of the weakness of the bonds that link the particles together, granular flows are defined by the interplay between these bonds and external loads – among which, gravity. While granular media constitute countless human-made and natural materials, predicting and controlling their behavior remains a challenge. This increases hazards from natural phenomena (avalanches, pyroclastic flows) and can be ecologically and economically damaging (e.g., sub-optimal efficiency of industrial powder handling processes).

We study the packing and flowing behavior of granular materials in microgravity. By understanding how granular media behave when gravitational acceleration is reduced, we can isolate the effect of particles' weight from intrinsic granular properties. Freed from gravity, competing microscopic forces that govern granular matter can be highlighted, providing a ground-truth to model their flow behavior. Primary activities of space exploration missions also rely on identifying the transition at which a granular material shifts behavior from

solid-like to fluid-like (its un-jamming transition), and once flowing, on predicting its rheology. Typical applications in space include building large structures and habitat, processing regolith for *in-situ* oxygen and metals production, or motorized exploration of asteroids and planetary surface.

Jamming describes the transition between the flowing state, in which the granular fabric undergoes plastic deformation, and the jammed state, where a stable contact network can withstand a certain amount of stress without large-scale reorganization, akin to a solid [1]. The jamming transition happens at a finite packing density, φ_J . It is indicated by a sudden rise in the number of contact per particle – and macroscopically, a sudden rise of the material's effective viscosity.

The packing density at jamming has been shown to vary with the gravitational acceleration, both in 2D [2] and 3D [3]. For the latter, experiments consisting of a piston rising through a granular medium, conducted on parabolic flights, showed that the jamming transition happens at lower density in microgravity than on-ground under Earth gravitational acceleration, g_E : $\varphi_J(g_\mu) < \varphi_J(g_E)$.

Granular rheology experiments have also been conducted in microgravity. Murdoch *et al.* [4, 5], using a Taylor-Couette geometry on parabolic flight (without stress measurement), found that the sec-

ondary radial displacement field is driven by a gravity-induced gradient, hence disappearing in microgravity. A similar setup including stress measurement was used by Bossis *et al.* [6] to study dilute to dense systems of iron beads (1 mm and 2 mm), confirming the classical scaling argument by Bagnold [7], $\sigma \propto \dot{\gamma}^2$, but finding prefactors largely exceeding expectations. Generally, rheological studies in microgravity have reported increased peak shear strength [8] and friction angles [9–11] compared to terrestrial conditions. Classical soil mechanics experiments adapted to partial- and microgravity also find increased dilation as gravity decreases [10, 11].

Smaller-scale experiments employing devices like hourglasses [12–18], rotating drums [13, 19–21], fluidized bed [22], or avalanche setups [13], consistently report lower packing densities and increased prominence of cohesive forces: powders that flow readily under Earth gravity exhibit cohesive behavior in low gravity, leading to aggregation and cluster formation which hinder flow [22–24].

An antagonist effect has also been reported. Lower gravitational acceleration reduces the confining pressure applied to a granular bed. On a sandy soil, it means that at shallow depth, the uppermost layer of soil is a dust-like, easily deformable material: the strength and soil’s bearing capacity are reduced [25, 26]; the first centimeters of penetration test require low effort [27, 28], and in avalanche flows, the fluid-like state can be prolonged [29], giving the impression of an easily flowing, fluid-like material.

This twofold effect complicates predictions of granular behavior outside of Earth gravitational field, which had severe consequences in the past. During the Apollo 15 Moon mission, astronauts lost hours of extravehicular activity (EVA) struggling to insert a core sampling penetrator into the lunar soil [30]. In 2009, the Mars rover Spirit was abandoned after six years of loyal services because it got embedded in soft granular soil, after all attempts at rescuing maneuvers failed [31]. More recently, the HP3 Mole penetrator of NASA’s InSight Mars lander failed to penetrate the Martian soil below 37 cm [32], a much shallower depth than planned. In future crewed missions, such misprediction could have catastrophic effects, notably risking astronauts’ safety.

We present a series of experiments in microgravity, where the effective gravitational acceleration, g , tends to zero, $g_\mu := g \rightarrow 0$. We investigate experimentally the influence of gravitational acceleration

on:

- (i) the packing fraction at which the granular jamming transition occurs;
- (ii) the rheology of the granular media under shear.

We use a simple experimental setup to first fluidize, then compress a granular packing until jamming. The packing density at jamming, φ_J , is measured at a given gravitational acceleration, g . Then, the granular material is subjected to shear, also under the given g , while measuring shear stress, τ , and variations in normal stress, $\Delta\sigma$. The same experiments are reproduced in microgravity and on-ground (g_E). We access microgravity using the two types of drop towers available at the Center of Applied Space Technology and Microgravity (ZARM) (Bremen, Germany), namely, free fall with catapult system [33] and active (guided) [34–36] drop towers.

We first describe the methods, notably focusing on the in-house developed experimental setup and the platforms used to conduct microgravity experiments. We then present our results on the packing density at jamming. Using fluidization to reinitialize our packing, we also observe the effect of gravity on the fluidization behavior. We then present our results on the rheology of granular materials in microgravity. Finally, we discuss how both changes in φ_J and granular rheology observed in microgravity can be understood in a common framework.

II. METHODS

A. Experimental procedure

The experimental procedure consists of the following (*cf.* Figure 1):

- (0) Before the start of the experiment, the material is fluidized to reinitialize a reproducible, low density packing.
- (1) The material is compressed by a piston until the pressure reaches the value p_J . The exact position of the piston is measured by an optical distance sensor, and used to calculate the volume occupied by the material, and in turn the packing fraction at jamming, $\varphi_J(g)$.
- (2) Once compressed, the mechanical (rheological) properties of the jammed material are probed by imposing shear through rotation of the inner cylinder. The piston is not at fixed position but can move slightly up and down

to accommodate for packing reorganization, while imposing a normal stress.

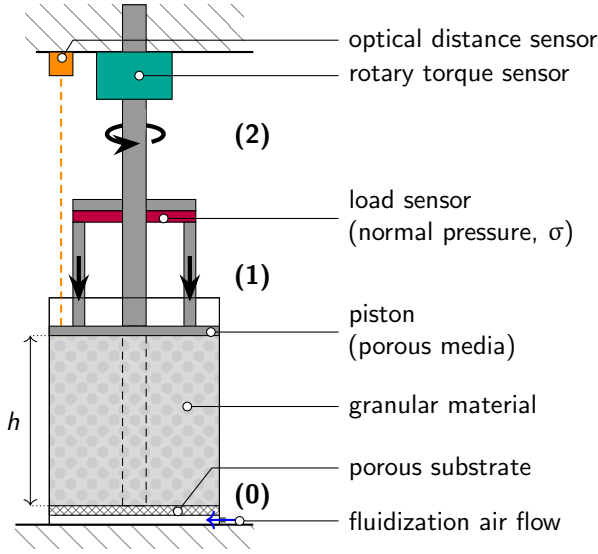


Figure 1: Schematic of experimental setup. The basic experiments conducted consist of (1) compression and (2) shear of a granular material. Data recording devices are: an optical distance sensor (orange) to measure the piston's height, h ; a rotary torque sensor (green) to measure shear stress, τ ; a normal load sensor (red) to estimate normal pressure changes, $\Delta\sigma$, due to the material's expansion or densification.

The experimental setup is shown in Figure 2. It comprises three main components: a fluidization system, a ring-shaped piston for compression, and a Taylor-Couette geometry rheometer (two coaxial cylinders with the inner cylinder rotating). The setup can slide opened to be divided into two parts, allowing for easy change of the granular material.

The piston is controlled by a linear actuator (BE069-3 from *Befenybay*), and connected to a normal load sensor. Values from the load cell (in kg) are converted into normal pressures, σ .

Once in contact with the powder bed, the piston position, h , gives the volume occupied by the material, from which we calculate its global packing fraction. The piston position is recorded by a triangulation laser distance sensor (OMom30-L0100.HV.TXN, Baumer), which has a precision of 1 μm . This sensor is selected based on the previously identified difference between φ_J on Earth and in microgravity [3], which, applied to our setup's scale, is expected to be approximately 0.1 mm.

During the compression test (measurement (1)), the jamming point is indicated by the halt of the piston and sudden rise of pressure. The vertical pressure at which the piston is stopped is empirically fixed at $p_J = 888 \text{ Pa}$. Note that for our

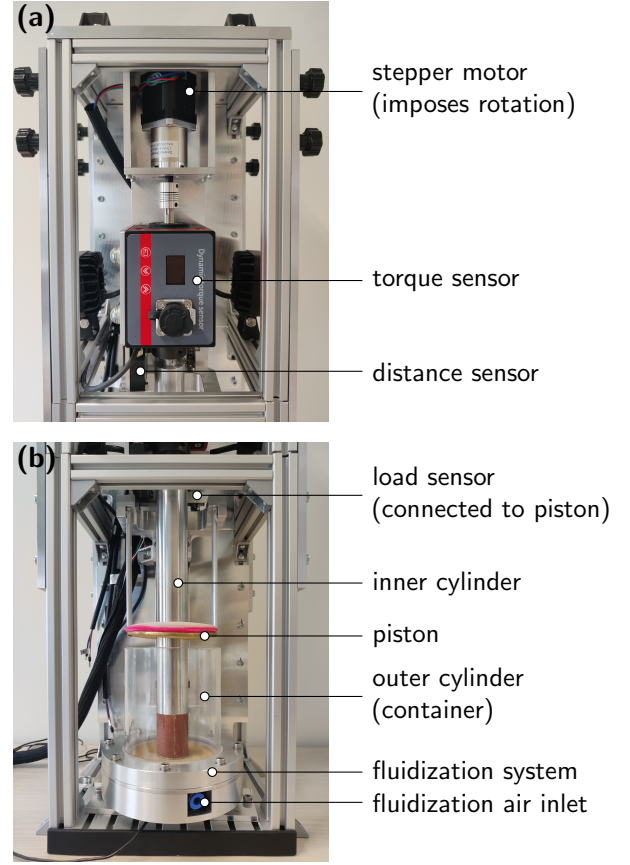


Figure 2: Picture of experimental setup. (a) Upper and (b) bottom part of the setup. The full setup is placed inside a capsule to undergo microgravity experiments, in the drop tower or in the GraviTower Bremen (GTB).

purpose – comparing the packing fraction at which jamming occurs under Earth and microgravity conditions – the exact pressure value is less critical than ensuring consistency in the experimental procedure across both environments. To account for the piston assembly's own weight, the measured load at time $t = 0$ is used as an offset (corresponding to the start of descending of the piston, at the same g as the experiment will take place).

To ensure quasi-static compression, the piston speed is fast at first (2.5 mm s^{-1}), then becomes slower as the pressure increases. It slows down to 0.75 mm s^{-1} once the normal pressure reaches 674 Pa. These values are determined empirically.

During the subsequent shear test (measurement (2)), the piston has the freedom to slightly move up and down to give space to the granular material to reorganize. This is implemented by a spring linking the piston to the linear actuator (see Fig. 3). A load cell is placed between the actuator (fixed during measurement (2)) and the spring, to capture compaction or dilation of the granular medium during shear. Variations in normal pressure, $\Delta\sigma$,

are given in regard to the normal pressure at the onset of shear.

B. Piston and packing fraction at jamming

The piston assembly, as shown in Figure 3, fulfills three functions: compressing the granular material into a jammed state; ensuring reliable particle containment during fluidization and launch, while letting the air-flow out; protecting the load cell from overload during hypergravity phases. A T-shaped component, mounted on the linear actuator, shields the load cell from excessive force by maintaining a ~ 0.1 mm gap below the load cell, where it is attached to the spring (see “protective gap” in Fig. 3). A U-shaped component connects the piston to the load cell via a spring. To prevent particle leakage, the piston itself features a sandwich structure: a sintered copper filter at the base permits airflow during fluidization, while a flannel ring, enclosed by a plastic ring, enhances sealing efficiency.

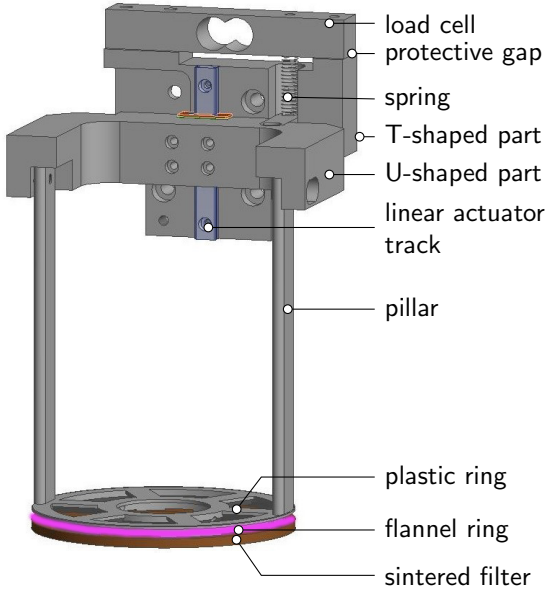


Figure 3: Piston assembly. The T-shaped structure protects the load cell from hypergravity-induced overload. The U-shaped connector transmits force between the load cell and the piston through a spring. The piston features a layered sealing system: a sintered copper filter allows airflow, a flannel ring prevents particle leakage, and a plastic ring maintains alignment.

The packing fraction is calculated via

$$\varphi_J = \frac{4m}{\rho_b \pi (d_c^2 - d_i^2) h} \quad (1)$$

where m is the mass of the granular sample; ρ_b is the bulk density of the material composing the granular particles; $d_c = 84$ mm is the diameter of

the container (outer) cylinder, and $d_i = 30$ mm is the diameter of the inner cylinder. h is the piston position; it is calculated taking as reference the bottom of the container, such that it represents the height occupied by the granular material.

C. Experimental uncertainty

The experimental uncertainty of the packing fraction determines whether the conclusions from our experiments are statistically relevant. Each variable in Eq. 1 is measured independently; absolute uncertainties are given in Table 1. The global experimental uncertainty of φ_J is calculated according to the simplified propagation of uncertainty [37]. The maximum absolute uncertainty is found to be 0.0061, corresponding to a relative uncertainty of 1%.

Table 1: Absolute uncertainty on each experimental variable. The values recorded here are used in the calculation of the experimental uncertainty.

	variable	unit	absolute uncertainty
ρ_b	material bulk density	kg m ⁻³	10
d_c	container outer diameter	m	10 ⁻⁴
d_i	inner cylinder diameter	m	10 ⁻⁴
h	piston position	m	10 ⁻⁶
m	material sample mass	kg	7 · 10 ⁻⁶

D. Air-fluidization

An air-fluidization system is installed to erase the stress history of the granular media before each experiment. Figure 4 shows a section view of the fluidization system.

A sealing ring is held in place by two metal pieces screwed together, holding the container cylinder and a porous filter with 35 μ m pore size; it creates a homogeneous gas flow in the container for uniform fluidization. To ensure proper centering of the inner cylinder, a cylindrical pocket is carved into the filter, fitted to the inner cylinder diameter.

E. Rheology

The second phase of the experiment consists of probing the mechanical (rheological) properties of

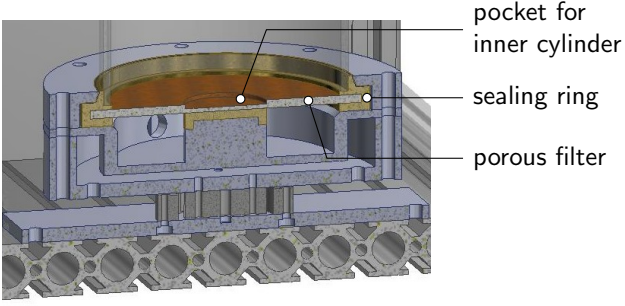


Figure 4: Section view of the fluidization system. This assembly is placed at the bottom the experimental setup, as indicated in Fig. 2.

the material. This is achieved by applying shear through the rotation of the inner cylinder (see Figs. 1 and 2). The piston is not moved up before the onset of shear, but the setup is designed such that the piston, connected to the structure via two springs, can move slightly up and down (*cf.* Sec. II.B and Fig. 3).

The inner cylinder rotation is controlled independently by a stepper motor (17HS19-1684S-PG100 from *Stepper-Online*) of maximum torque 4 N m. The rotational stepper motor features a 100:1 gear-box to ensure ample torque provision.

The inner cylinder is rotated at constant speed of 4.3 rpm in every rheology experiment presented. Translated to shear rate (assuming Newtonian behavior), the material is sheared at $\dot{\gamma} = 10^{-1} \text{ s}^{-1}$.

The rotational torque sensor (ATO-TQS-DYN-200 from ATO) used to measure torque, M , has a capacity range of -0.1 N m to 0.1 N m , with a precision of $100 \text{ } \mu\text{N m}$ and accuracy of $30 \text{ } \mu\text{N m}$. Sandpaper is used at the bottom of the inner cylinder to avoid slippage (coarse grit 60, typical rugosity $\sim 250 \text{ } \mu\text{m}$); it covers a height $L = 35 \text{ mm}$.

The shear stress, τ , is calculated from the recorded torque, M , as

$$\tau = \frac{M}{2\pi h r_i}. \quad (2)$$

The variations in normal pressure from that at the onset of shear, $\Delta\sigma$, are recorded throughout each shear test.

F. Microgravity platforms

Microgravity conditions (g_μ) – that is, effective weightlessness obtained by free fall under Earth gravity – are provided by the ZARM drop towers in Bremen (Germany). Two different systems are used:

- The GraviTower Bremen (GTB), a relatively short active drop tower [34, 35]. In the GTB,

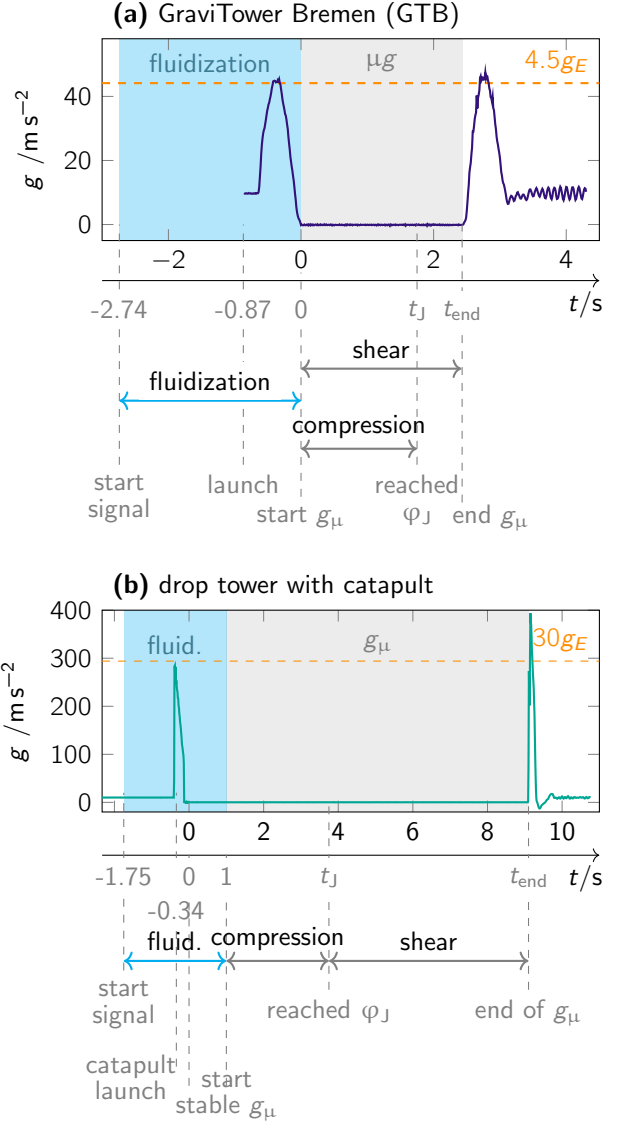


Figure 5: Acceleration in the experimental capsule and corresponding experiment timeline. (a) Acceleration *versus* time during a GTB experiment. Shear and compression experiments are conducted independently. (b) Acceleration during a drop tower experiment with catapult. Compression, then shear are conducted consecutively. Note that the instant at which the jamming point is reached, t_J , is not time-controlled but controlled by the pressure imposed by the piston.

the experimental capsule is actively guided to match the speed variations of free fall. It provides 2.3 s of microgravity.

- The (passive) drop tower with catapult system, where the experiment describes a parabola in vacuum, providing 9.3 s of effective microgravity [33].

Typical acceleration profiles measured on either of the platforms are provided in Figure 5. We also provide the nominal timing for all types of experiment conducted.

Data collection in microgravity is constrained by the limited availability of experimental platforms. For reference, each experiment is also performed under Earth gravity (g_E); ground repetitions follow a microgravity run as closely as possible, to ensure the same conditions.

G. Materials

Two granular materials are used. The first one is composed of monodispersed polystyrene spherical particles of diameter $d = 1$ mm (polystyrene bulk density $\rho_{PS} = 1.05 \text{ g cm}^{-3}$), with relatively smooth surface.

The second granular material is also composed of monodispersed spherical polystyrene particles, but with much smaller diameter $d = 80 \mu\text{m}$. They also exhibit relatively smooth surface, but as smaller particles, they exhibit higher interparticle cohesion [18, 42]. This material is from the manufacturer *Dynoseeds* under the label *Microbeads*; their flow-behavior is characterized in Refs. [38, 39].

III. RESULTS

A. Jamming transition density

The compression experiment was conducted three times in microgravity using the GTB, with the 1 mm diameter particles.

Snapshots from a representative experiment are shown in Figure 6 (video 1339 in Supplementary Material). Three independent repetitions are presented in Figure 7(a-c). Fluidization ceases as gravity approaches g_μ , at which point the piston starts its downward motion for compression.

A short waiting time is introduced after fluidization to allow the packing to relax. At the onset of microgravity, a brief negative acceleration typically occurs, causing expansion of the granular packing and upward motion of some particles (visible in Sup. Mat. video 1339; see also Fig. 6(b)).

For the sake of comparison, three exemplary datasets in Earth gravity, g_E , are provided in Fig. 8. A total of ten independent repetitions of the experiment were conducted, as reported in Fig. 9(b).

In Figures 7 and 8, the piston's vertical position is normalized by its initial and final position, so that $\Delta z = 0$ is its starting position and $\Delta z = 1$ the position at which the packing jams; i.e., let h_0 be the starting height of the piston and h_J the height at which the packing jams, $\Delta z(h) = (h - h_0)/(h_J - h_0)$. Time is expressed either from

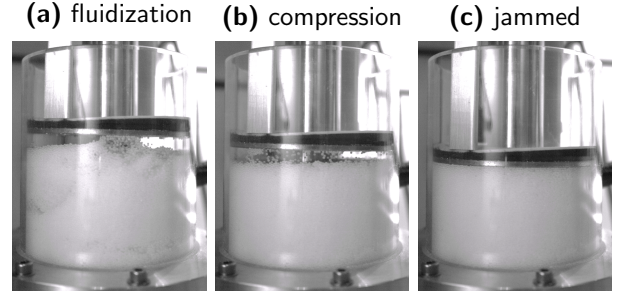


Figure 6: Screenshots from the control video during GTB experiment on 1 mm diameter polystyrene particles. After (a) fluidization, (b) the piston is lowered to compress the material until measuring a steep increase in normal pressure up to p_J , at which point (c) the piston is stopped as the material is considered jammed.

the start of microgravity (Fig. 7), or from the onset of piston's motion for ground experiments (Fig. 8).

A summary of the packing fractions measured in all experiments is presented in Fig. 9(a,b), corresponding to microgravity and ground-based conditions, respectively. Error bars indicate the experimental uncertainty associated with the measurement.

From Figure 9, we see that the jamming packing fraction, φ_J , is lower in microgravity than in terrestrial gravity on every repetition, with average values of $\langle \varphi_J^{g_\mu} \rangle = 0.587$ and $\langle \varphi_J^{g_E} \rangle = 0.606$.

To quantify variability within each dataset despite differing sample sizes, we calculate the coefficient of variation, c_v , defined as the ratio of the standard deviation to the mean, (also known as relative standard deviation). We find $c_v^{g_\mu} = 0.1\%$ and $c_v^{g_E} = 0.4\%$, indicating a larger dispersion in the measurements conducted under Earth gravity compared to microgravity, notwithstanding the unequal sample size and generally low variability.

B. Fluidization behavior

We use fluidization to reinitialize the granular packing before each repetition, erasing its stress history to ensure consistent initial conditions. Previous work by Born *et al.* [40] demonstrated that fluidization in microgravity leads to a homogeneous, fully mobilized state, in contrast to behavior observed under Earth gravity.

In the experiment described above (1 mm polystyrene beads fluidized during a GTB experiment, *cf.* Fig. 7 and Sup. Mat. videos), the launch phase induces an acceleration of approximately $4.5g_E$; fluidization is maintained throughout hypergravity and ceases at the onset of microgravity. A slight negative acceleration immediately following

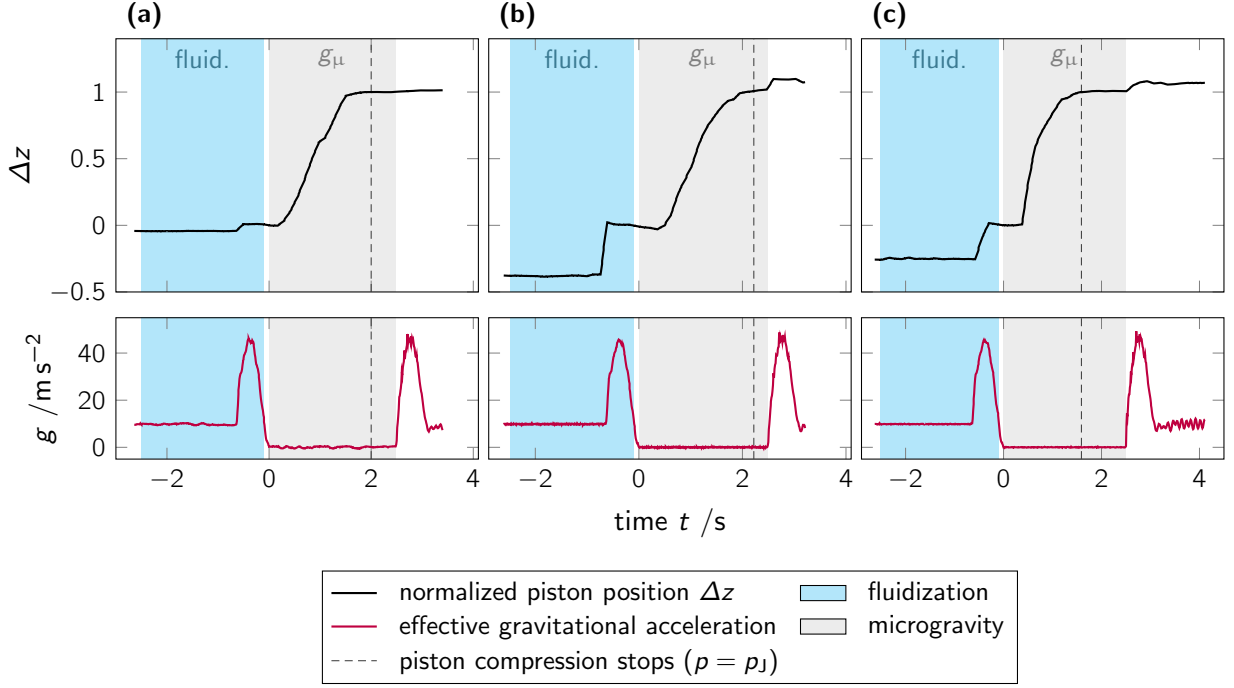


Figure 7: Normalized piston position variation up to the jamming point and effective gravitational acceleration during three GTB tests. The piston position, Δz , is normalized by its initial and final positions; g is the effective gravitational acceleration throughout a GTB test. All experiments shown here are conducted on the GTB with $d = 1$ mm spherical polystyrene particles. The piston stops when reaching p_J , indicated by a dashed line. Fluidization and microgravity and marked by shaded background (blue and grey, respectively).

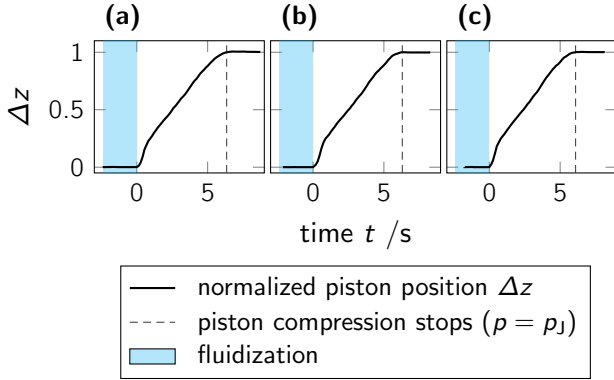


Figure 8: Normalized piston position variation up to the jamming point during tests in Earth gravity. The piston position, Δz , is normalized by its initial and final positions. All experiments shown here are conducted with $d = 1$ mm spherical polystyrene particles (note that three out of ten repetitions are shown here). The piston stops when reaching p_J , indicated by a dashed line. Fluidization is marked by blue shaded background.

the hypergravity phase further aids the granular bed expansion.

Here, we focus on the second experiment, which uses much smaller $80 \mu\text{m}$ polystyrene beads, in the drop tower with catapult. This exposes the capsule to an initial acceleration of almost 300 m s^{-2} ($\sim 30g_E$, cf. Fig. 5(b)), compacting the granular bed significantly under its own weight. Before,

during and for one second after this initial acceleration peak, the granular media is subjected to a fluidizing airflow at constant pressure $p = 0.1$ bar – identical to that used in ground-based fluidization. Screenshots of the key phases, captured by the control camera, are shown in Figure 10.

Note that in both experiments (GTB and drop tower), the same fluidization pressure is applied across all gravity regimes (Earth, hypergravity, microgravity). The purpose of fluidization in these experiments is not to investigate reduced-gravity fluidization *per se*, but to prevent packing compression by reinitializing the bed as acceleration decreased following the launch hypergravity phase.

As seen in Fig. 10(c), just after hypergravity and while the airflow persists in microgravity, the granular material does not exhibit individual particle agitation. Instead, the entire granular bed is displaced as a cohesive block, behaving more like a porous solid than a fluidized discrete medium. When compression starts, this block is pushed downward uniformly, without visible signs of particle motion.

Packing fraction data from this experiment are excluded from further analysis, as the observed compaction could not be attributed to the controlled piston compression alone, but rather to the substantial pre-compaction induced by launch acceleration.

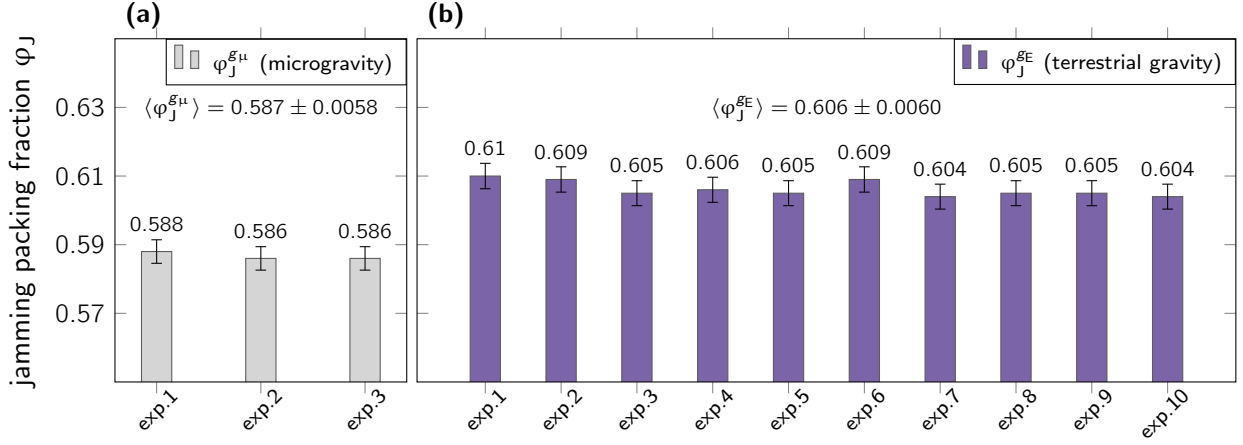


Figure 9: Global packing fraction at jamming, ϕ_J , for all microgravity and Earth gravity compression tests conducted. All experiments shown here are conducted with $d = 1$ mm spherical polystyrene particles; all microgravity experiments were conducted in the GTB. Error bars are the experimental uncertainty on the measurement. $\langle \phi_J \rangle$ are averages over each repetitions, given with the variance over all repetitions per g .

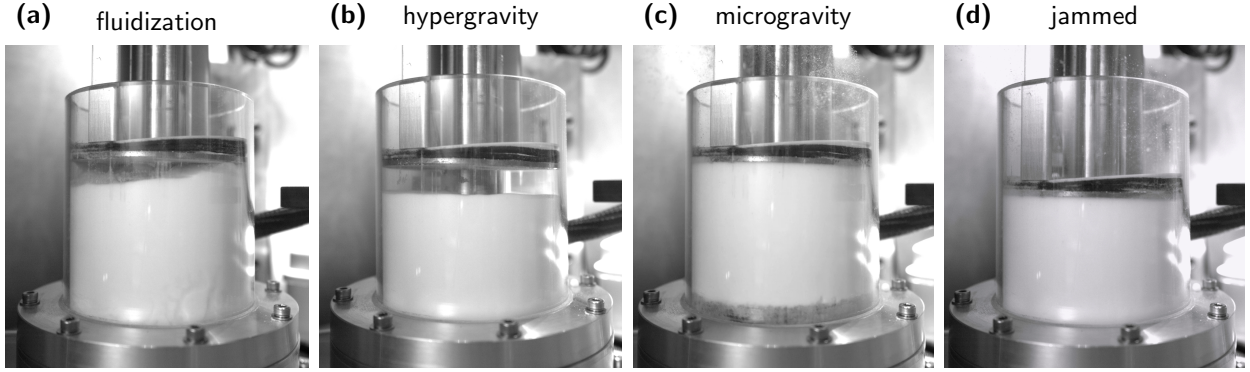


Figure 10: Screenshots from the catapult drop tower experiment. This experiment used $80 \mu\text{m}$ polystyrene particles. The granular bed is first fluidized (a), then it experiences an initial compaction due to launch-induced hypergravity ($\sim 30g_E$) (b); the fluidization is continued throughout hypergravity and for one second in microgravity. Once in microgravity, the entire bed is shifted upward as a block by the airflow (c). The piston then starts descending to compress the granular packing (d).

Nonetheless, this experiment illustrates the challenge of fluidizing highly cohesive powders in microgravity. Under Earth gravity, a balance between particle weight and upward airflow drag allows for a fluid-like, agitated state [40, 41]. In microgravity, however, the particles' weight being eliminated and cohesive forces dominating can reduce the effectiveness of air-fluidization in agitating the granular material, pointing to the need for further investigation into mechanisms of granular bed reinitialization in low- and microgravity.

These findings point to the need for further investigation into mechanisms of granular bed reinitialization in low- and microgravity environments. For long-duration experiments on orbital platforms (e.g., the international space station (ISS) and its successors), if air-fluidization is used for packing reinitialization, it should be supplemented with mechanical agitation to ensure effective disordering

to ensure reproducibility of the initial state.

C. Rheology

Two types of shear tests were conducted. First, four repetitions of shear experiments using fine polystyrene powder ($d = 80 \mu\text{m}$), performed in the GTB. The results are shown in Figures 11 for microgravity and 12 for the corresponding ground-based experiments. Second, an additional shear test was conducted in the drop tower with a catapult system with large polystyrene beads ($d = 1$ mm) (Figure 14(a)), and was subsequently reproduced on-ground (Figures 14(b-d)).

In both experimental configurations, the duration of microgravity – limited to seconds – does not allow the system to reach a steady state. In sheared granular materials, the relaxation times can be long, with steady state sometimes requir-

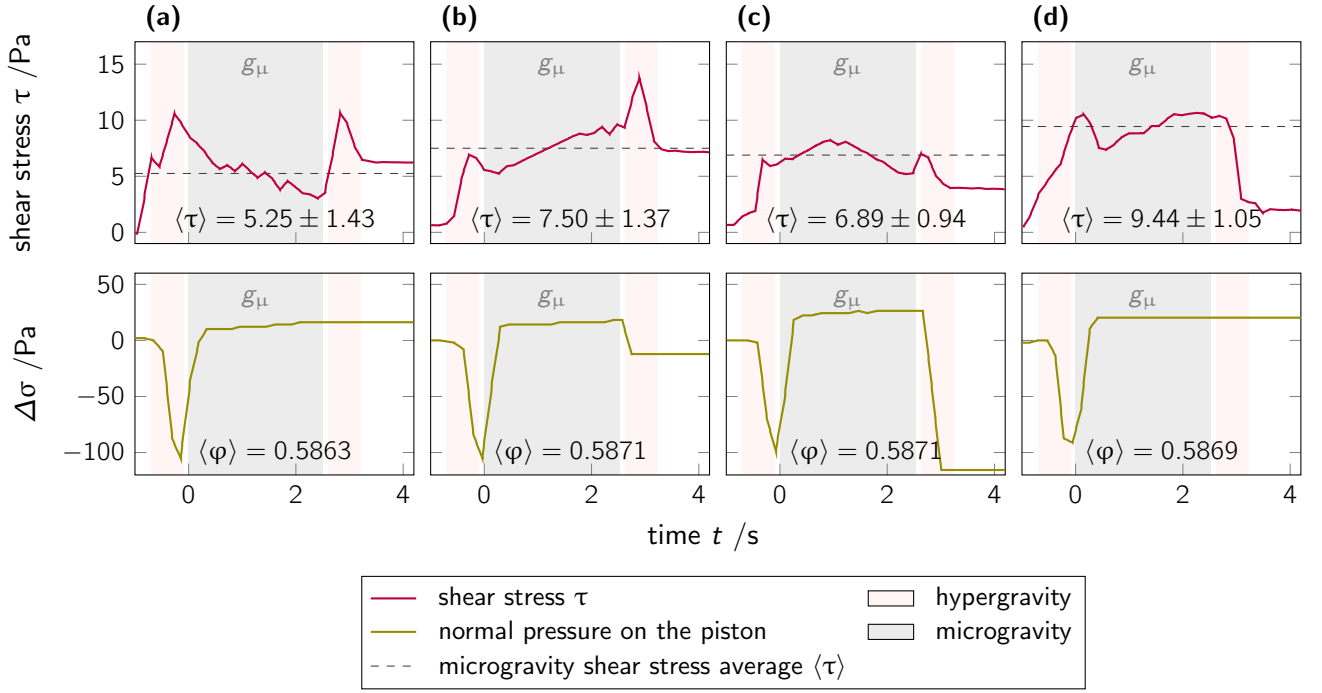


Figure 11: Shear stress τ and variations in normal pressure $\Delta\sigma$ for microgravity experiments conducted in the GTB. All experiments shown here are conducted with $80\ \mu\text{m}$ diameter polystyrene particles. Microgravity is marked by grey and hypergravity by red shaded background. Dashed lines mark the average shear stress $\langle \tau \rangle$ (numerical value and standard deviation for each measurement given in panel). The average packing density during the test, $\langle \phi \rangle$, are given in the bottom panels (also compiled on the microgravity period).

ing hours to establish, notably in Taylor-Couette shear geometry [41]. The microgravity platforms used here inherently constrain the duration of experiments, and are thus not suited for long-term behavior.

Figure 11 shows the results of the four shear tests conducted in the GTB. Each panel shows the shear stress, τ (upper plot) and the corresponding change in normal pressure, $\Delta\sigma$ (lower plot), relative to the baseline measured immediately before the start of the shear experiment (typically at $t = -1\text{ s}$). The normal pressure is not controlled but only measured; it provides information on whether the granular bed expands or compacts during shear (remember that the piston is mounted on a spring, *cf.* Figure 3). The onset of inner cylinder rotation happens at $t = -1\text{ s}$; microgravity starts at $t = 0$. The material is sheared throughout the hypergravity phase, such that the shear stress recorded corresponds to the stress needed to maintain and not initiate shear in microgravity. The shaded grey area denotes microgravity; shaded red, hypergravity.

Shear stress measurements across the four microgravity experiments are relatively consistent, with an average shear stress over all repetitions of $\langle \tau \rangle_{g_\mu} = 7.27\text{ Pa}$ ($c_v^{g_\mu} = 24\%$). Temporal fluctuations within individual experiments account for

coefficients of variations between 11% and 27%, with no systematic trend of increase or decrease.

The normal pressure variations, $\Delta\sigma$, exhibits a sharp drop during the hypergravity phase prior to microgravity onset, reflecting the strong compaction of the granular bed under the combined influence of downward acceleration and shear. This is followed by a sudden expansion upon entering microgravity, leading to a consistent increase in normal pressure of approximately $+20\text{ Pa}$ across all repetitions.

These results can be compared to the corresponding experiments in terrestrial gravity (Figure 12). The shear stress values are on average lower than those measured in microgravity (although not consistently). Stress fluctuations are significantly larger within individual tests (c_v ranging from 38% to 49%), but similar when comparing the three repetitions ($c_v^{gE} = 23\%$). The normal pressure under Earth gravity remains either roughly constant or decreases (up to -40 Pa), indicating progressive densification of the packing under shear in Earth gravity.

Figure 13 shows the average shear stress in microgravity and Earth gravity using boxplots. It confirms that the average shear stress required to drive the flow is higher in microgravity than in Earth gravity, while stress fluctuations are higher

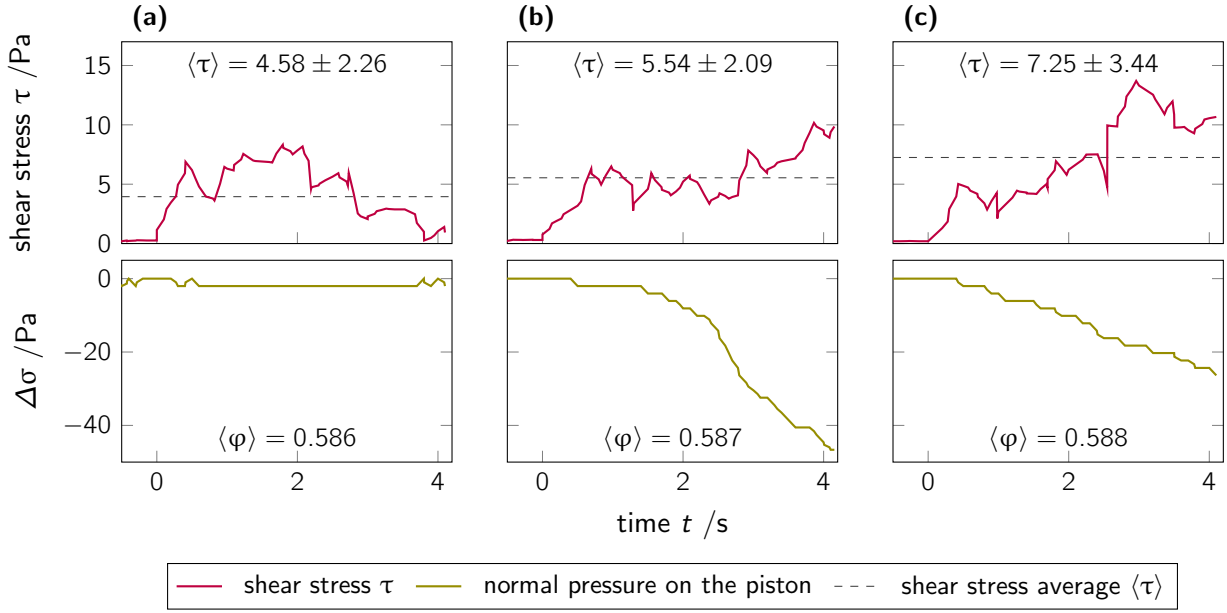


Figure 12: Shear tests conducted under Earth gravity with 80 μm diameter polystyrene powder. Graphs (a), (b) and (c) represent three repetitions of the same experiment. The upper panels show the shear stress *versus* time, as well as the average shear stress over the test, $\langle\tau\rangle$ (plotted as dashed line). The lower panels show the changes in normal pressure, $\Delta\sigma$, from the onset of shear (at $t = 0$). $\langle\phi\rangle$ is the average packing fraction over the test.

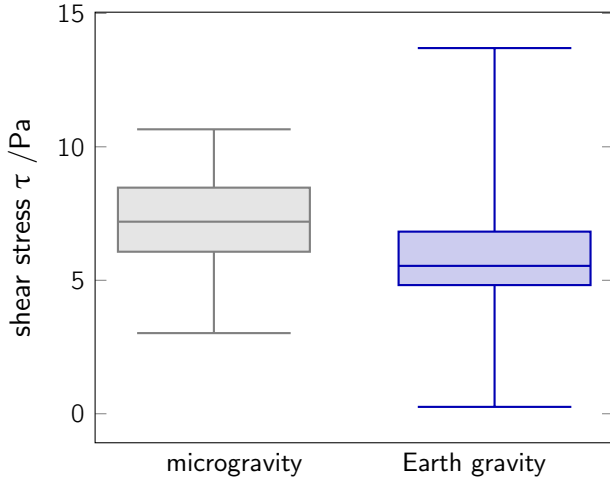


Figure 13: Statistics of shear tests conducted in microgravity and in terrestrial gravity with 80 μm diameter polystyrene powder. Boxplots use the same data as Figs. 11 and 12.

when terrestrial gravity is present.

This can be explained by the fact that under terrestrial gravity, the acceleration field supports the reorganization of the packing, facilitating flow. However, gravity also pulls the material down, forcing interparticle contacts with a finite normal stress. To be sheared, the system must overcome these frictional contacts, which can lead to stick-slip events, and in turn increased variations in shear stress, thus higher standard deviations.

The second set of shear experiments uses larger

particles ($d = 1\text{ mm}$, polystyrene), and is conducted in the drop tower with catapult (Figure 14(a)). In this configuration, shear is initiated only after the onset of microgravity. The average shear stress in microgravity reaches a notably high value of 42.15 Pa. After the initial increase, the standard deviation remains around 1 Pa, similar to the ones found in previous microgravity experiments (Fig. 11).

Three independent repetitions are reproduced in terrestrial gravity (Figure 14(b-d)). We find the average shear stress recorded on-ground to be lower than that in microgravity, with $\langle\tau\rangle_{g_\mu} \approx 4\langle\tau\rangle_{g_E}$. This significant increase in measured stress confirms the trend previously observed: granular materials subjected to shear in microgravity can exhibit markedly higher resistance to flow than under Earth gravity conditions, even for large, relatively non-cohesive particles.

IV. DISCUSSION

Our compression experiment show that jamming transition appears at lower density in microgravity than on-ground: $\varphi_J(g_\mu) < \varphi_J(g_E)$, in agreement with previous work [3] conducted on parabolic flights. In these previous experiments, jamming was induced by a piston rising in a granular packing; we reproduce this result in compression, using larger particles (diameter 1 mm against 80 μm in Ref. [3]), and reinitializing the granular packing

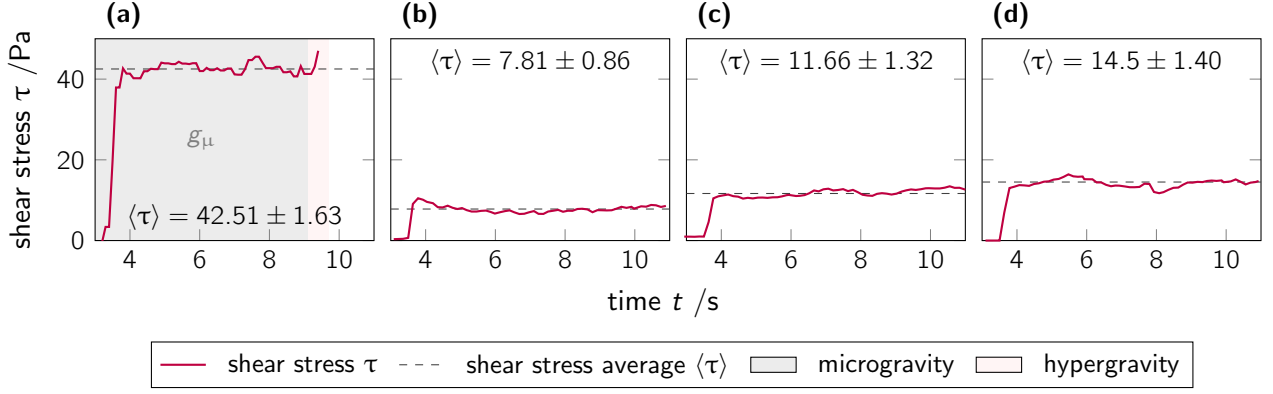


Figure 14: Shear stress versus time for drop tower shear test and corresponding individual ground test, for polystyrene particles of diameter $d = 1$ mm. Panel (a) shows drop tower test data; the light grey shading indicates microgravity, light red shading hypergravity. Panels (b), (c) and (d) show the corresponding data for terrestrial gravity. The dashed lines show the time averaged data, $\langle \tau \rangle$.

by fluidization between each test. Here, we find a deviation of approximately 3% between $\varphi_J(g_\mu)$ and $\varphi_J(g_E)$ (against 2% in Ref. [3]). These deviations are small but statistically significant – as confirmed below – and hold practical relevance in the context of granular material processing, where slight changes in packing can markedly influence granular behavior.

Given the limited number of experimental data points available under microgravity, each measurement is particularly valuable. To evaluate the relation between φ_J and g , we apply a statistical correlation test to the datasets microgravity and terrestrial gravity datasets. All φ_J values used are reported in Figure 9; gravitational acceleration is treated as the independent variable, and φ_J as the dependent variable. For the experimental dataset, the Pearson correlation coefficient between φ_J and gravitational acceleration is 0.9721, indicating a very highly positive correlation between gravitational accelerations and φ_J . This supports our conclusion that the packing fraction at jamming, φ_J , depends on the gravitational acceleration.

Let us now consider the behavior of the material under shear. Across both materials and microgravity platforms, we consistently observe that a higher shear stress is required to deform the granular material under microgravity compared to Earth gravity (*cf.* Figs. 11, 12, 13, 14).

We rationalize these finds using results from Murdoch *et al.* [4], who showed that in microgravity, Taylor-Couette shear flow does not exhibit the secondary (radial) flow field typically present under gravity. In other words, under microgravity, particle rearrangement is restricted to the primary shear direction, with no aid from gravity to facilitate reorganization.

On Earth, gravity acts as a supplementary load, normal to the shear direction. This not only provides additional confinement, but also introduces motion perpendicular to the shear plane, which can help particles bypass jamming configurations. The absence of this mechanism in microgravity may therefore lead to enhanced resistance to shear, reflected in the increased torque measurements.

Besides, in microgravity, the absence of significant gravitational loading fundamentally alters the balance of forces acting on each particle. On Earth, the weight of individual particles contributes to the overall confining pressure, effectively overcoming weak interparticle cohesive forces – such as van der Waals or electrostatic cohesive forces – in most dry granular systems [42]. However, in microgravity, the gravitational load is minimized or eliminated, allowing cohesive forces to dominate particle interactions. As a result, the granular assembly behaves more like a weakly bound solid than a loosely packed fluid [18]. This shift in force balance also explains the consistently higher shear stresses observed in microgravity experiments: the system behaves more like a cohesive medium, requiring greater stress to initiate and sustain shear. Furthermore, the predominance of cohesion over weight reduces particle sliding and rearrangement.

A closer look at the evolution of the normal pressure during shear (Fig. 15) also shows that in microgravity, the granular packing expands over time, whereas on Earth, it densifies. This contrast is again consistent with the absence of gravity-induced settling in microgravity: once particles are agitated by shear, there is no preferential direction to fall into interstitial voids and compact the granular packing. On Earth, however, gravity forces particles to rearrange into denser configura-

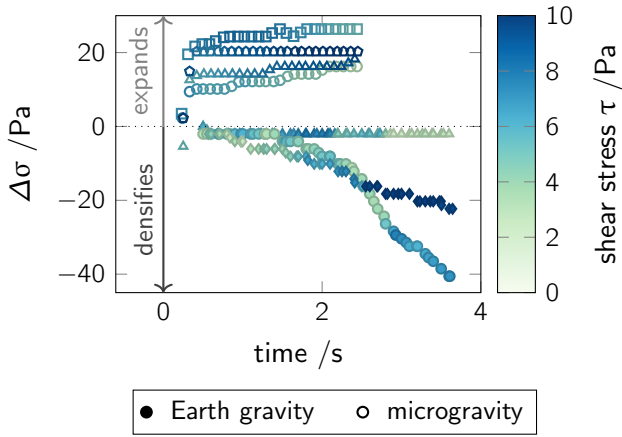


Figure 15: Evolution of normal pressure and shear stress in Earth- and microgravity. The normal pressure change, $\Delta\sigma$, applied by the granular media to the piston.

tions during shear (as well as during compression), promoting densification.

This difference in behavior is also evident in the variability of the shear stress measurements (Fig. 13). For the fine polystyrene powder ($d = 80\ \mu\text{m}$), standard deviations of shear stress are systematically larger in Earth gravity tests than in microgravity (Figs. 12 (g_E) and 11 (g_μ), respectively). This increased variability is present both within individual repetitions and across repetitions. Gravity introduces an additional constraint and load-bearing direction, thereby amplifying local heterogeneities and stick-slip behavior.

Our observations align with findings by Featherstone *et al.* [28], who report more frequent stick-slip events at higher gravity. In contrast, granular media in microgravity were described as more *fluid-like*, with smoother and more continuous deformation of the granular fabric. This reduced variability in our microgravity data supports such interpretation: without the gravity-induced normal stress, frictional contact networks might be less prone to intermittent locking and sudden release (stick-slip).

Note, however, that in this study we used only relatively smooth, spherical particles; increasing surface friction, roughness, and/or introducing angular or interlocking shapes might reveal additional features of granular flow behavior in microgravity.

To summarize, we propose the following hypotheses to rationalize our results:

- **Minimization of potential energy:** In a gravitational field, particles tend to move to lower positions to minimize their potential energy, provided the packing geometry allows for it. This leads to a net densification of the

granular medium, as gravity drives downward reorganization of particles.

- **Gravity as a supplementary load and loading direction:** Gravity provides a secondary force field, adding a normal stress component to the applied stress tensor [3, 4]. This might promote plastic rearrangement by helping particles overcome friction and escape local jamming. On Earth, such gravity-induced secondary flows assist reorganization; their absence in microgravity might result in increased resistance to shear.
- **Reduced variability and stick-slip dynamics in microgravity:** Gravity enhances local heterogeneities and promotes intermittent stick-slip behavior [28]. In contrast, granular media in microgravity behave more fluid-like, with smoother, more continuous deformation, possibly due to reduced frictional locking in the absence of gravity-induced normal loading.
- **Enhanced role of cohesive forces in microgravity:** Interparticle cohesive forces (e.g., van der Waals, electrostatic, capillary) are typically much weaker than gravity; in microgravity, they are no longer dominated by particles' weight and thus become predominant [18, 24, 38]. These cohesive interactions resist particle separation, which might make granular materials more difficult to shear.

V. CONCLUSION

In this study, we investigated the influence of gravity on granular density at jamming and shear response, through a series of experiments conducted in microgravity and terrestrial gravity conditions. We used an in-house developed setup combining compression and shear (Taylor-Couette shear geometry), on two microgravity platforms: the GTB (smaller active drop tower) and the drop tower with catapult at the ZARM in Bremen, Germany. For materials, spherical, monodispersed polystyrene particles of two sizes were employed ($d = 80\ \mu\text{m}$ and $d = 1\ \text{mm}$).

Across all tests and materials, we consistently found that the packing fraction at jamming, φ_J , depends on the gravitational acceleration, with granular packing jamming at lower packing density in microgravity than in Earth gravity: $\langle\varphi_J\rangle_{g_\mu} = 0.587$ and $\langle\varphi_J\rangle_{g_E} = 0.606$, respectively. This result is

statistically significant, as evidenced by a Pearson correlation coefficient of 0.9721.

Regarding granular rheology in microgravity, we find that higher shear stress is required in microgravity than in terrestrial gravity, with $\langle\tau\rangle_{g_\mu} = 7.27$ Pa in GTB experiments and $\langle\tau(g_E)\rangle = 5.79$ Pa in terrestrial gravity. We also find reduced variability in microgravity measurements, indicating smoother, more continuous flow.

We propose different hypothesis of gravity-dependent mechanisms to explain our results. On Earth, gravity not only imposes an additional load normal to the shear plane, but also enables particle rearrangement through a secondary flow field. In contrast, in microgravity, the absence of a secondary flow field might lead to reduced plastic reorganization and increased resistance to shear. Furthermore, cohesive forces – generally negligible compared to particles’ weight – become dominant in microgravity, further impeding particle rearrangement and enhancing shear resistance.

Together, our results reveal how gravity affects not only the magnitude of stresses required to shear granular media, but also the underlying particle dynamics. These insights are important for predicting and controlling granular behavior in low gravity environments, with direct implications for planetary exploration, *in-situ* resource utilisation (ISRU), and spacecraft operations involving regolith or granular flows.

Future work should aim to build on these findings through more systematic and comprehensive experiments (as proposed for example by Duffey *et al.* [43]), including longer-duration experiments, and using a broader variety of granular materials; this includes varying particle shape, size distribution, surface roughness, and cohesive properties, to better isolate and quantify the influence of each factor. Low- and microgravity experiments provide an opportunity to expose microscopic interactions typically masked by Earth’s dominant gravitational force. Ultimately, such efforts aim to develop a general granular rheology model that remains valid under reduced gravity.

REFERENCES

- [1] R. P. Behringer and B. Chakraborty, “The physics of jamming for granular materials: a review”, *Reports on Progress in Physics* **82**, 012601 (2018).
- [2] S. Dorbolo, T. Scheller, F. Ludewig, G. Lumay, and N. Vandewalle, “Influence of a reduced gravity on the volume fraction of a monolayer of spherical grains”, *Phys. Rev. E* **84**, 041305 (2011).
- [3] O. D’Angelo, A. Horb, A. Cowley, M. Sperl, and W. T. Kranz, “Granular piston-probing in microgravity: powder compression, from densification to jamming”, *npj Microgravity* **8**, 48 (2022).
- [4] N. Murdoch, B. Rozitis, K. Nordstrom, S. F. Green, P. Michel, T.-L. de Lophem, and W. Losert, “Granular convection in microgravity”, *Phys. Rev. Lett.* **110**, 018307 (2013).
- [5] N. Murdoch, B. Rozitis, S. F. Green, T.-L. de Lophem, P. Michel, and W. Losert, “Granular shear flow in varying gravitational environments”, *Gran. Matter* **15**, 129–137 (2013).
- [6] G. Bossis, Y. Grasselli, and O. Volkova, “Granular rheology in zero gravity”, *Journal of Physics: Condensed Matter* **16**, 3279 (2004).
- [7] R. A. Bagnold, “Experiments on a gravity-free dispersion of large solid spheres in a newtonian fluid under shear”, *Proceedings of the Royal Society of London. Series A, Mathematical and Physical Sciences* **225**, 49–63 (1954).
- [8] S. Sture, N. C. Costes, S. N. Batiste, M. R. Lankton, K. A. AlShibli, B. Jeremic, R. A. Swanson, and M. Frank, “Mechanics of granular materials at low effective stresses”, *Journal of Aerospace Engineering* **11**, 67–72 (1998).
- [9] K. A. Alshibli, S. Sture, and N. C. Costes, “Constitutive and stability behavior of soils in microgravity environment”, *AIP Conference Proceedings* **504**, 246–252 (2000).
- [10] J. P. Marshall, R. C. Hurley, D. Arthur, I. Vlahimic, C. Senatore, K. Iagnemma, B. Trease, and J. E. Andrade, “Failures in sand in reduced gravity environments”, *J. Mech. Phys. Solids* **113**, 1–12 (2018).
- [11] K. Karapiperis, J. P. Marshall, and J. E. Andrade, “Reduced gravity effects on the strength of granular matter: dem simulations versus experiments”, *Journal of Geotechnical and Geoenvironmental Engineering* **146**, 06020005 (2020).

- [12] S. Dorbolo, L. Maquet, M. Brandenbourger, F. Ludewig, G. Lumay, H. Caps, N. Vandewalle, S. Rondia, M. Mélard, J. van Loon, A. Dowson, and S. Vincent-Bonnieu, “Influence of the gravity on the discharge of a silo”, *Granular Matter* **15**, 263–273 (2013).
- [13] A. Brucks, L. Richter, J.-B. Vincent, and J. Blum, “Effect of reduced-gravity conditions on the flowability of granular media”, in *Earth & space 2008* (), pp. 1–8.
- [14] P. Reiss, P. Hager, A. Hoehn, M. Rott, and U. Walter, “Flowability of lunar regolith simulants under reduced gravity and vacuum in hopper-based conveying devices”, *Journal of Terramechanics* **55**, 61–72 (2014).
- [15] P. G. Hofmeister, J. Blum, and D. Heißelmann, “The flow of granular matter under reduced-gravity conditions”, *AIP Conference Proceedings* **1145**, 71–74 (2009).
- [16] S. Ozaki, G. Ishigami, M. Otsuki, H. Miyamoto, K. Wada, Y. Watanabe, T. Nishino, H. Kojima, K. Soda, Y. Nakao, M. Sutoh, T. Maeda, and T. Kobayashi, “Granular flow experiment using artificial gravity generator at international space station”, *npj Microgravity* **9**, 61 (2023).
- [17] I. P. Madden, S. Muruganandam, A. Misraoui, O. Gries, J. Kollmer, O. D’Angelo, and S. Sinha-Ray, “Behaviors of lunar regolith simulants under varying gravitational conditions”, *npj Microgravity* (2025).
- [18] O. Gaida, O. D’Angelo, and J. E. Kollmer, *To flow or not to flow? the granular bond number to predict clogging in low gravity*, 2025.
- [19] S. P. Klein and B. R. White, “Dynamic shear of granular material under variable gravity conditions”, *AIAA Journal* **28**, 1701 (1990).
- [20] A. Brucks, T. Arndt, J. M. Ottino, and R. M. Lueptow, “Behavior of flowing granular materials under variable g ”, *Phys. Rev. E* **75**, 032301 (2007).
- [21] M. G. Kleinhans, H. Markies, S. J. de Vet, A. C. int Veld, and F. N. Postema, “Static and dynamic angles of repose in loose granular materials under reduced gravity”, *Journal of Geophysical Research: Planets* **116**, 10.1029/2011JE003865 (2011).
- [22] R. Williams, R. Shao, and R. A. Overfelt, “The flowability of fine powders in reduced gravity conditions”, *Granular Matter* **10**, 139–144 (2008).
- [23] F. Elekes and E. J. R. Parteli, “An expression for the angle of repose of dry cohesive granular materials on earth and in planetary environments”, *Proceedings of the National Academy of Sciences* **118**, e2107965118 (2021).
- [24] S. G. Love, D. R. Petit, and S. R. Messenger, “Particle aggregation in microgravity: informal experiments on the international space station”, *Meteoritics & Planetary Science* **49**, 732–739 (2014).
- [25] A. Singh, V. Magnanimo, K. Saitoh, and S. Luding, “The role of gravity or pressure and contact stiffness in granular rheology”, *New Journal of Physics* **17**, 043028 (2015).
- [26] P.-Q. Mo, G. Zhou, F. Gao, and R. Li, “Bearing capacity of surface circular footings on granular material under low gravity fields”, *Journal of Rock Mechanics and Geotechnical Engineering* **13**, 612–625 (2021).
- [27] E. N. Slyuta, “Physical and mechanical properties of the lunar soil (a review)”, *Solar System Research* **48**, 330–353 (2014).
- [28] J. Featherstone, R. Bullard, T. Emm, A. Jackson, R. Reid, S. Shefferman, A. Dove, J. Colwell, J. E. Kollmer, and K. E. Daniels, “Stick-slip dynamics in penetration experiments on simulated regolith”, *The Planetary Science Journal* **2**, 243 (2021).
- [29] T. Shinbrot, N.-H. Duong, L. Kwan, and M. M. Alvarez, “Dry granular flows can generate surface features resembling those seen in martian gullies”, *Proceedings of the National Academy of Sciences* **23**, 8542–8546 (2004).
- [30] National Aeronautics and Space Administration (NASA), *Apollo 15 mission report*, Technical Report 19720021182 (NASA, 1971).
- [31] R. A. Kerr, “Mars rover trapped in sand, but what can end a mission?”, *Science* **324**, 998 (2009).
- [32] T. Spohn, T. L. Hudson, L. Witte, T. Wippermann, L. Wisniewski, B. Kedziora, C. Vrettos, R. D. Lorenz, M. Golombek, R. Lichtenheldt, M. Grott, J. Knollenberg, C. Krause, C. Fantinati, S. Nagihara, and J. Grygorczuk, “The InSight-HP3 mole on Mars: lessons learned from attempts to penetrate to depth in the Martian soil”, *Advances in Space Research* **69**, 3140–3163 (2022).

- [33] P. von Kampen, U. Kaczmarczik, and H. J. Rath, “The new drop tower catapult system”, *Acta Astronautica* **59**, 278–283 (2006).
- [34] T. Könemann, U. Kaczmarczik, A. Gierse, A. Greif, T. Lutz, S. Mawn, J. Siemer, C. Eigenbrod, P. von Kampen, and C. Lämmerzahl, “Concept for a next-generation drop tower system”, *Advances in Space Research* **55**, 1728–1733 (2015).
- [35] A. Gierse, U. Kaczmarczik, A. Greif, H. Selig, P. von Kampen, T. Könemann, and C. Lämmerzahl, “A fast and self-acting release-caging-mechanism for actively driven drop tower systems”, *Microgravity Science and Technology* **29**, 403–414 (2017).
- [36] A. Gierse, T. Könemann, P. von Kampen, and M. Avila, “The gravitower bremen pro – experiences with a next-generation drop tower system”, in 73rd international astronomical congress (iac) (International Astronomical Federation (IAF), Sept. 2022), pp. 1–5.
- [37] H. H. Ku, “Notes on the use of propagation of error formulas”, *Journal of Research of the National Bureau of Standards* **70C**, 262 (1966).
- [38] O. D’Angelo, F. Kuthe, S.-J. Liu, R. Wiedey, J. M. Bennett, M. Meisnar, A. Barnes, W. T. Kranz, T. Voigtmann, and A. Meyer, “A gravity-independent powder-based additive manufacturing process tailored for space applications”, *Additive Manufacturing* **47**, 102349 (2021).
- [39] O. D’Angelo, “Effect of cohesion and friction on granular flow”, [preprint] (2025).
- [40] P. Born, J. Schmitz, and M. Sperl, “Dense fluidized granular media in microgravity”, *npj Microgravity* **3**, 27 (2017).
- [41] O. D’Angelo, M. Sperl, and W. T. Kranz, “Rheological regimes in agitated granular media under shear”, *Phys. Rev. Lett.* **134**, 148202 (2025).
- [42] O. Pouliquen, “Powders and cohesive granular media: a rheological perspective”, *Rheologica Acta* **64**, 195–207 (2025).
- [43] C. Duffey, M. Lea, and J. Brisset, “Measuring regolith strength in reduced gravity environments in the laboratory”, *Review of Scientific Instruments* **96**, 065201 (2025).

ACKNOWLEDGEMENTS

We would like to extend gratitude to Achim Sack and Walter Pucceanu for their help in creating the experimental setup, as well as the ZARM personnel, in particular Dieter Bischoff.

This work was supported by the German Aerospace Center (DLR) Space Administration with funds provided by the German Federal Ministry for Economic Affairs and Climate Action (BMWK) under grant number 50WM2342A and through access to the ZARM drop tower facilities and engineering support under the project name “*J versus g*”.

O. D’A. acknowledges financial support from the Emerging Talents Initiative (ETI) program 2023 by the Friedrich-Alexander-Universität (FAU) Erlangen-Nürnberg, and from the French National Centre for Space Studies (CNES) under the CNES fellowship 24-357.

DATA AVAILABILITY STATEMENT

The data that support the findings of this study are available from the corresponding author upon request.

SUPPLEMENTARY MATERIAL

The supplementary videos show the granular compression tests conducted in microgravity, in the GTB, using polystyrene spherical particles of diameter 1 mm). Each video includes, in the lower-left corner, a graph of the measured acceleration during the experiment, with a vertical line progressing in sync with the video. The original recording frame rate is 300 fps. The videos are slowed down 10 times, playing at 30 fps. Videos included are:

- **Video 1339** (Fig. 7(a));
- **Video 1359** (Fig. 7(b));
- **Video 1408** (Fig. 7(c)).